LUND UNIVERSITY
Faculty of Science

The Magnetic Characterization of Iron-Chrome Oxide Nanoparticles

Angga Virdian

Thesis submitted for the degree of Master of Science
Project duration: 10 months

Supervised by Rasmus Westerström and Maria Messing.

Department of Physics
Division of Synchrotron Radiation Research
May 2018

Popular Abstract

The understanding of magnetism has always been a substantial achievement of humankind. Magnetic materials are used everywhere in the society, from data storage in hard drives to magnetic resonance imaging (MRI) in hospitals. Magnetic materials are also essential components in technologies that convert electric power into motion or vice versa, and thus play a key role in the replacement of fossil fuels in vehicles and the transition to renewable energy sources.

Nanomagnetism is a branch of physics that deals with the magnetic behavior of the nanoscale objects such as metallic nanoparticles. Magnetic nanoparticle has been applied in to various field. Iron oxide is an example of versatile material that works in MRI imaging, data storage and in cancer treatment.

Magnetic nanoparticles could also be used as the building blocks for next generation of permanent magnetic materials for green technologies such as electric vehicles and wind turbines. This thesis is a part of a larger research project with the aim of studying magnetic nanoparticles consisting of different magnetic elements, so-called alloys. The long-term goal of this project is to use nanoparticles to produce magnetic materials with performance rivaling today's strongest magnets but using cheaper and more sustainable materials. To determine the magnetic properties of nanoparticles, it is essential that they are not nearby and thereby influence each other. The goal of this thesis is to explore the possibility of studying low coverage of alloyed magnetic nanoparticles that are sufficiently far apart to not influence each other. This will be achieved by depositing the low coverage on a substrate with low magnetic signal and measuring the properties of the particles with an ultra-sensitive magnetometer, a so-called superconducting quantum interference device.

Abstract

In this thesis, the intrinsic magnetic characteristic of 10 nm FeCr oxide nanoparticles is studied. The nanoparticles is produced using the method of Spark discharge generation. Scanning electron microscope (SEM) is used to characterize the size distribution and coverage of deposited particle. Magnetic characterization is carried out using a magnetometer equipped with superconducting quantum interference device (SQUID). Temperature and external magnetic field dependent measurements are done to study the magnetic properties. The image of surface reveals the majority of nanoparticle has the size of 9 to 12 nm. At this size the particle can be assumed single-domain state. The particle coverage is considered low with one particle per 10404 nm^2, thereby minimizing interparticle magnetic dipole-dipole interactions. Magnetic characteristics reveal the magnetic moment dynamic as the variation of thermal energy. The magnetic characterization reveals that the nanoparticles are superparamagnetic with a blocking temperature of 51 K. At a temperature of 2 K, the nanoparticles are in a blocked state and exhibit magnetic hysteresis similar to a ferromagnetic system. The future of magnetic nanoparticle lies on the alloyed particle that consists of two or more elements. This research act as a preliminary study of alloy using Iron chrome oxide as test system before advancing to the more complex system.

Acknowledgement

I would like to express my gratitude to Rasmus Westerström and Maria Messing as the supervisor and co-supervisor of my thesis research supervisor for the patient guide and the opportunity to do research in an exciting field of Nanomagnetism. During the proceeding of this research a lot of constructive critiques and useful discussion.

I also would like to thank the soon-to-be doctor in physics, Calle Preger and Claudiu Bulbucan. Our discussion about nanoparticle and magnetic data processing is helpful to the progression of the research.

My special gratitude for the all friends, family, and comrades from all across the world that support me in this arduous journey. Their companionship, courage, kindness, and warmth keep me going through the hardship and beyond.

Contents

Glossary

DMA Differential mobility analyzer. 13

FeCr Iron Chrome. 12

SDG Spark discharge generation. 12–14

SEM Scanning electron microscope. 14–17, 19, 25

SQUID Superconductor quantum interference device. 12, 17–19, 22

TEM Tunneling electron microscope. 14

Chapter 1

Introduction

Transition metal element and their magnetic behavior has been extensively studied. Some of the material is known to have spontaneous magnetization, addressed as ferromagnetic or ferrimagnetic. In the last decades study of material has shifted to further down the scale due to advancement of nanofabrication. Nanoparticles of these materials can exhibit vastly different magnetic behavior with its bulk counterpart. A widely known example of the magnetic nanoparticle is Iron oxide, that exhibit different magnetic depending on the size [1]. As the size goes down, new magnetic behavior such as superparamagnetism can be observed. For Iron oxide nanoparticles, this state of material is proven versatile for application in various field from biological imaging, to advance nanomedicine and cancer treatment [2, 3, 4].

Magnetic materials used in applications are usually alloys and oxides having complex structures with different magnetic elements. Next generation of high-performing magnets may not be single-phase alloys or compounds, but composites tailored on the nanoscale to achieve the desired properties for a specific application [5].

This thesis is a part of a larger project with the aim of producing and studying complex alloyed magnetic nanoparticle systems. To study the intrinsic properties of these systems, it is important to minimize interactions between the nanoparticles. The goal of this thesis is to explore the possibility of studying low coverage of FeCr oxide nanoparticles.

In this chapter, the key concept in magnetism will be introduced along with basic theory about magnetic behavior in nanoparticle. Chapter 2 will be focused on the fabrication and characterization method . Chapter 3 is going to described the nanoparticle size and distribution study along with and the magnetic data analysis. Chapter 4 contain the conclusion of the research project.

1.1 Magnetic Dipoles

A magnetic dipole consists of a north pole and a south pole as shown at figure 1.1. The magnetic dipole generates a magnetic field that extends from the north pole to the south pole. The strength of the magnetic field is related to the magnetic dipole moment represented by a vector directed from the south pole to the north pole.

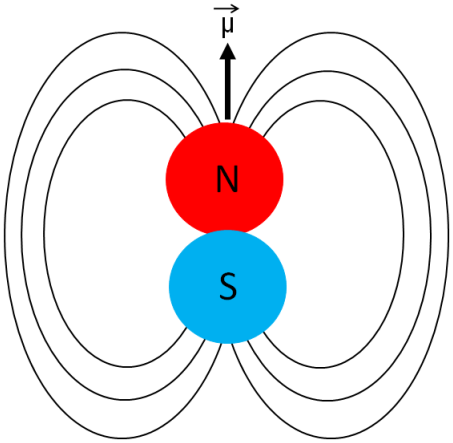

Figure 1.1: The magnetic moment dipole.

Magnetization in the atom can be predicted using the current loop model and quantum mechanics concept. The electron in atom occupy a certain energy level corresponding to an atomic orbital. The wave functions of an atomic orbital contain the probability of finding the electron at a certain position around the nuclei. The probability per unit time of finding the electron in an orbital with an angular moment $L > 0$ has an angular dependence and is in a sense analogous to the current loop in Figure 1.2. Since the orbital angular momentum of the electron is quantized we can expect the magnetic moment to also be quantized.

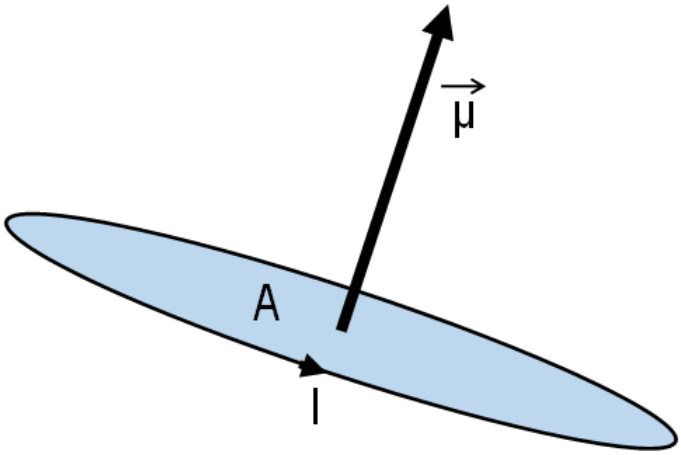

Figure 1.2: The magnetic moment of current in the loop.

The magnetic momentum in an atom due to electron orbital movement can be written as:

$$\begin{aligned} |\mu_L| &= -\frac{e}{2m_e}|\hat{L}| \\ &= -\mu_B\sqrt{l(l+1)}. \end{aligned} \tag{1.1}$$

Where μ_B is Bohr magneton and l is orbital angular quantum number.The electron

also has an intrinsic orbital moment called spin which generates a magnetic moment μ_S. The spin magnetic momentum is:

$$\begin{aligned} |\mu_S| &= -\frac{1}{2m_e} g_e |\hat{S}| \\ &= -\mu_B g_e \sqrt{s(s+1)}. \end{aligned} \tag{1.2}$$

Where s is the spin quantum number and g_e is gyromagnetic ratio. The total magnetic moment by electron is the addition of angular momentum contribution and the spin part, and can be written as:

$$\mu = \mu_L + \mu_S \tag{1.3}$$

Magnetic moments can interact with each other with respect of their distance. This interaction is called magnetic dipole-dipole interaction, each dipole will interact with magnetic field produced by neighboring atom's magnetic moment. One can calculate the potential energy of this interaction.

$$E = \frac{\mu_0}{4\pi r^3}[\vec{\mu_1} \cdot \vec{\mu_2} - \frac{3}{r^2}(\vec{\mu_1} \cdot \vec{r})(\vec{\mu_2} \cdot \vec{r})] \tag{1.4}$$

The long-range dipole-dipole interaction can be significant for magnetic nanoparticles. To study the intrinsic properties of magnetic nanoparticles, it is crucial to minimize the dipole-dipole interactions. Here, low coverage sample is used to minimize this effect.

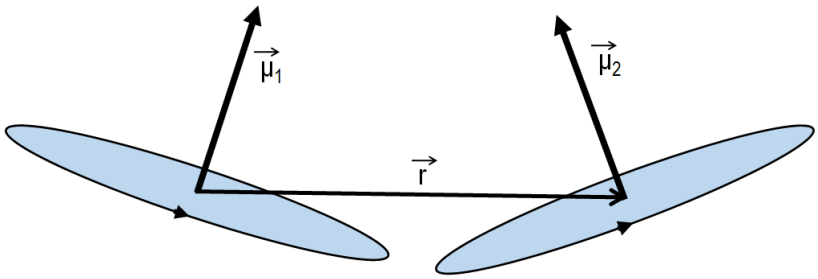

Figure 1.3: The geometry of magnetic dipole interaction.

The interaction of the atomic magnetic moment $\vec{\mu}$ and a magnetic field $\vec{B}$ is given by the Zeeman energy

$$E_{Zeeman} = -\vec{\mu} \cdot \vec{B} \tag{1.5}$$

The Zeeman interaction is the reason a magnetic material can be magnetized in the presence of an external magnetic field.

1.2 Paramagnet and Ferromagnetic Material

The behavior of magnetic moment determine the response of material when subjected to external magnetic field. For this research project the property of material is predicted to make a transition between paramagnet and ferromagnet. It is beneficial to briefly revisit and determine the difference between them.

The magnetic moments in a paramagnetic material do not have a preferred orientation in the absence of an applied external magnetic field [Figure 1.4 (a)]. When a magnetic field is applied, the Zeeman interaction favors an alignment of the magnetic moments parallel to the applied field. Opposing this alignment is the thermal energies in the system that randomly flips the magnetic moments [1.4 (b)]. Only when the Zeeman energy is much larger than the thermal energies are all magnetic moments aligned along the field direction [1.4 (c)].

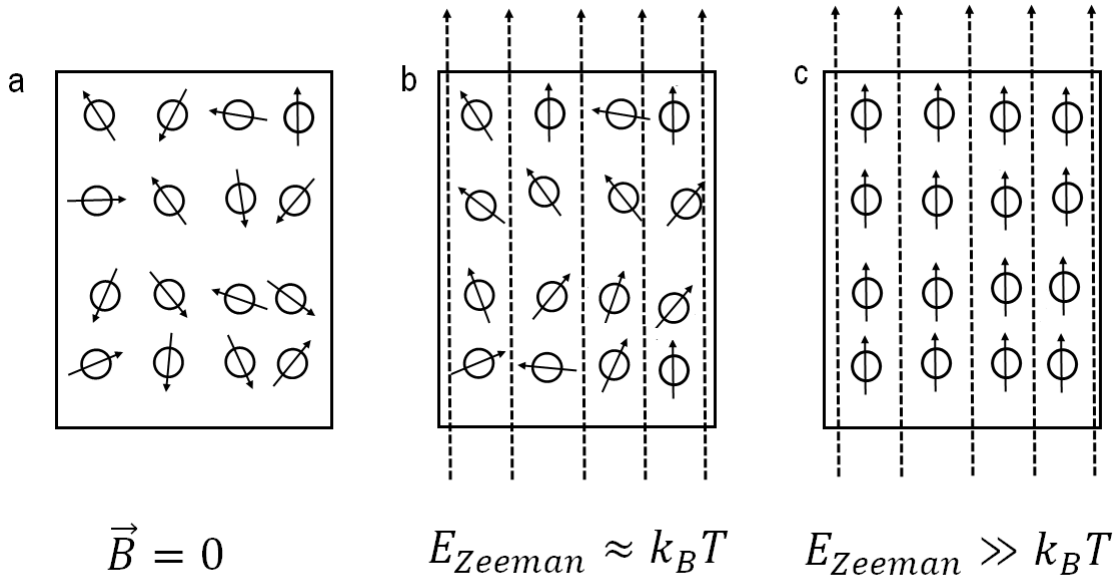

Figure 1.4: The Paramagnetic material response on various external magnetic field.

The magnetization of this material is explained by the Langevin function $L(x)$.

$$\begin{aligned} M &= N\mu L(x) \\ L(x) &= \coth x - \frac{1}{x} \\ x &= \frac{\mu B}{k_B T} \end{aligned} \tag{1.6}$$

where N is the total number of atoms, the total magnetic moment of atom μ, the external magnetic field B and temperature T. Figure 1.5 shows the calculated magnetization of FeCr oxide nanoparticle with 10 nm diameter at various temperature, see appendix A.

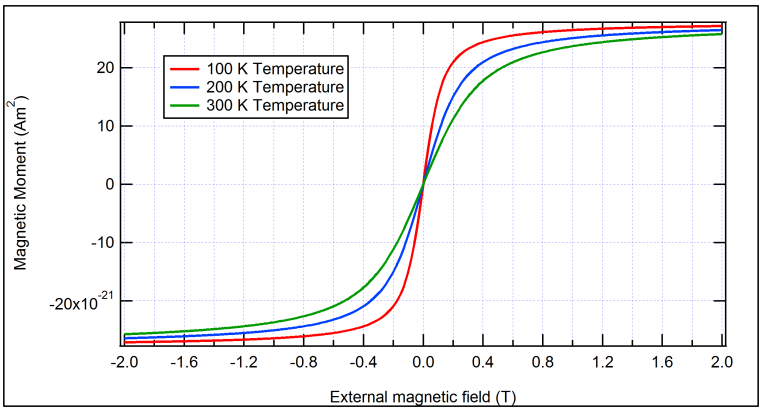

Figure 1.5: The Langevin function that describe the magnetization as effect of external magnetic field and temperature for of FeCr oxide nanoparticle with a diameter of 10 nm.

The ferromagnetic has the property of ordering in magnetic momentum, so all of its magnetic momenta align in the same direction. The result is this material exhibit magnetization without any external field. Magnetic ordering can also result in an antiparallel alignment of magnetic moments. In a Ferrimagnet, magnetic moments from different ions align with opposite directions. Because the opposing magnetic moments have different magnitudes, the system still has a non-vanishing net magnetization [Figure 1.6 (b)]. Magnetite Fe_3O_4 is a ferrimagnet where the opposing magnetic moments from the Fe^{3+} ions cancel each other and what is left is a moment of 4 μ_B from the Fe^{2+}. Antiferromagnet on the other hand experience the same antiparallel alignment, but the magnitude of the opposing moments is equal and therefore bring the net magnetization to zero. An example of an antiferromagnet is Cr_2O_3.

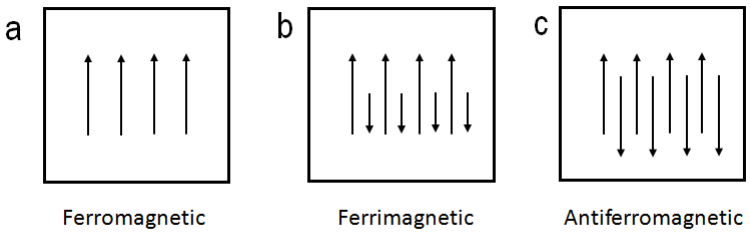

Figure 1.6: Magnetic ordering in ferromagnet, ferrimagnet and antiferromagnetic.

Ordering in ferromagnetic material raises an interesting question, what if such thing is subjected to an external magnetic field. At the beginning the magnetic moment does not have any preferred orientation, and then an external magnetic field is applied and eventually makes the system reach saturation. When external field is reduced to zero, the remaining alignment results in a remanent magnetization M_r. The remanent magnetization thus gives the degree of magnetic ordering the system can sustain in the absence of an external magnetic field. As the external field change to the opposite direction, the magnetization will eventually vanish, and the field when this happens is called the coercive field B_c. Finally, when the external field is

large enough, all moments are aligned in the opposite direction, and the system has reached its negative saturated magnetization. If the external field is reversed ones more, the system will eventually reach its positive saturated magnetization again following a different but symmetric path. A magnetization curve like this that do not follow the same path is said to exhibit hysteresis.

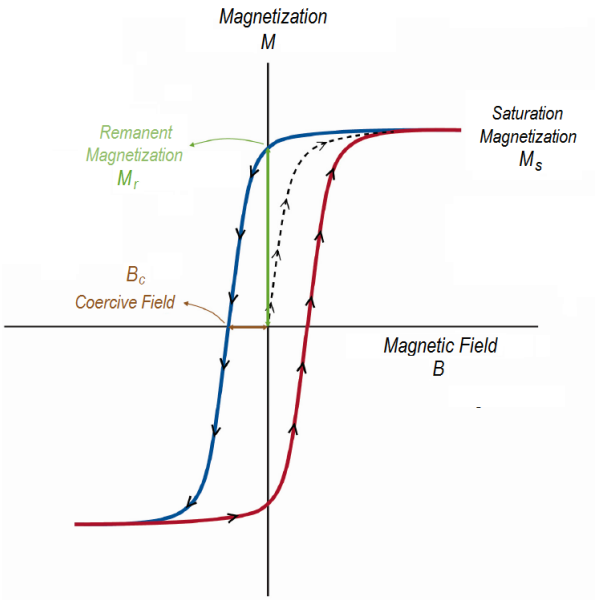

Figure 1.7: Magnetic response of ferromagnetic material when subjected to external magnetic field [6].

1.3 Spin-Orbit Coupling and Magnetocrystalline Anisotropy

The orbital and spin magnetic moments can couple together by the so-called spin-orbit coupling, figure 1.8 help visualize this phenomenon using a simple atomic model that consists of electron that revolves around nucleus on its orbital and also spinning on its axis. The magnetic field produced by the revolution of electron H_{orb}, interact with magnetic moment of electron spin μ_S similar to the dipole-dipole interaction described in section 1.1.

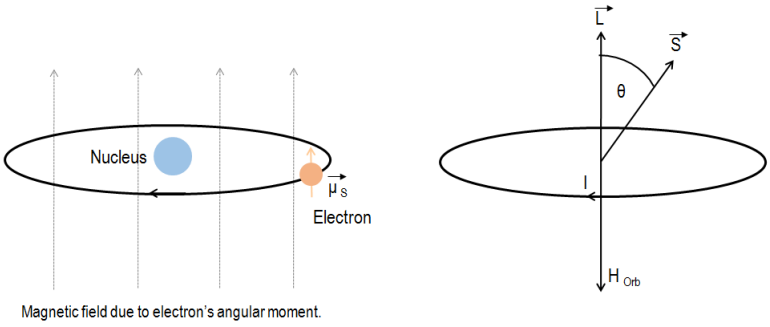

Figure 1.8: Spin-orbit coupling illustration; the simplified picture of the system (left) and the vector representation vector.

In solid however, atoms is confined in ordered structure. The angular part of the electron wavefunctions with $l > 0$ in the atom has an anisotropic shape and direction in space and corresponds to the probability of finding the electron in a particular region in space. Orbitals pointing towards neighboring atoms in the crystal have higher energy due to Coulomb repulsion than orbitals that point where there are no atoms. The variation in energy due to the crystal structure is called crystal field interaction. The consequence is that there exist directions defined by the crystal structure where the orbital angular magnetic moment μ_L has the lowest energy. The spin magnetic moment μ_S is then locked in the same direction through the spin-orbit coupling. These directions of lowest energy are called easy magnetic axis [7].

One can map out the anisotropy in energy as a function of system's magnetic moment angle, figure 1.9 shows this relation. The energy it takes to rotate the magnetic moment along the magnetic easy axis is given by KV where K is the anisotropy constant given in units of Jm^{-3} and V the volume. External energy is able to induce the magnetic moment of nanoparticle to flip between their easy axis provided it has enough energy to overcome the anisotropy barrier.

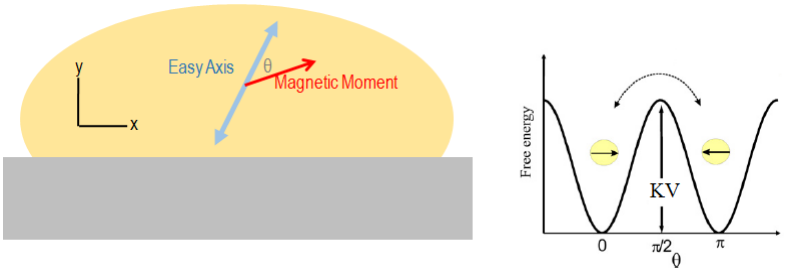

Figure 1.9: The anisotropy in space and its relation with energy [8].

1.4 Magnetic Domain

Macroscopic permanent magnets do not have a single magnetic easy axis. Instead, empirical observations indicate that the material is segmented into smaller regions called domains, each with a specific magnetic easy axis as shown in figure 1.10 (a). The critical size when material form a single domain is given by the equation below [7, 9].

$$D_{cr} = \frac{72\sqrt{AK}}{\mu_0 {M_s}^2} \tag{1.7}$$

A is exchange energy, the K anisotropy constant, μ_0 vacuum permeability, and M_s saturation magnetization.

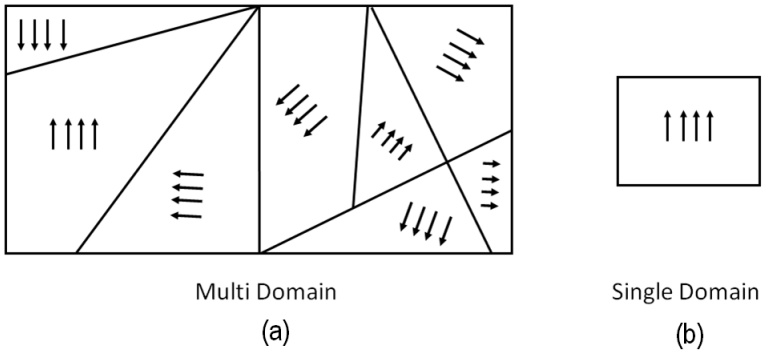

Figure 1.10: Multi domain and single domain illustration, arrow represent the direction of easy axis for particular domain.

1.5 Iron Oxide

Iron has tendency to bond with oxygen to form Fe_2O_3 or Fe_3O_4. In a semi-classical picture, the crystal field interaction prevents the electrons to freely orbiting the nucleus and the orbital magnetic moment is largely quenched. As a result, the magnetic moment of the Fe ions comes almost solely from the unpaired spins in the $3d$ valence shell. However, there is still a small orbital moment that couples to the electron spin and give rise to magnetic anisotropy. Figure 1.11 shows the electron configuration of Fe^{+2} ion, the magnetic moment of the atom raise from the unpaired spin in valence shell, which has the magnitude of $4\mu_B$. The critical size for magnetite Fe_3O_4 nanoparticles is 76 nm [10]. Here we are investigating $(Fe_{0.85}Cr_{0.15})_3O_4$, though the parameters entering equation 1.7 will differ, one can assume that 10 nm particle in this study will be single domain.

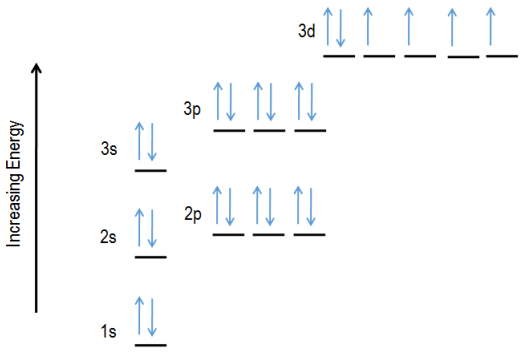

Figure 1.11: Electron configuration of Fe^{+2} ion.

Chapter 2

Experimental and Characterization Method

Iron-based alloy nanoparticles are structures consisting of the combination of iron and other metal, sometimes more than one kind, that is confined in nanoscale. For this particular research project, the material of interest is the FeCr oxide. The future magnetic material might consist of complex metallic alloy, where the interaction between different metallic elements will lead to various functional properties. The study of simple metallic alloy, like FeCr oxide will provide some insight on the magnetic characteristics in alloy system, something that is needed before more complex alloy can be studied.

The aerosol method named Spark discharge generation (SDG) is used to produce a uniformly sized nanoparticle. The spark discharge generator consists of two opposing electrodes connected to a power supply, and the nanoparticles are formed by evaporation and condensation of material from the electrodes. The formed nanoparticles are size selected in a differential mobility analyzer and deposited onto a substrate placed inside an electrostatic precipitator. The concentration of particles on the substrate can be controlled, but the particles are randomly distributed on the substrate. By depositing a low concentration of particles one can minimize interaction between particles. Scanning electron microscope is employed to confirm the size of nanoparticle and study its distribution. Lastly, the working principle of an ultrasensitive magnetometer equipped with superconductor quantum interference device (SQUID) and its capability of detecting magnetic field are explained.

2.1 Spark Discharge Generation

The huge interest of the scientific community to study material in nanoparticle form calls for a robust particle generation technique. The spark discharge generation or SDG offers a great alternative of aerosol based method [11]. This technique uses spark discharge generation between to electrodes to evaporate electrode material and let that material condense into nanoparticles. Through a series of reshaping and size-selection steps the nanoparticles have a relatively uniform size distribution and can be deposited onto a substrate [12].

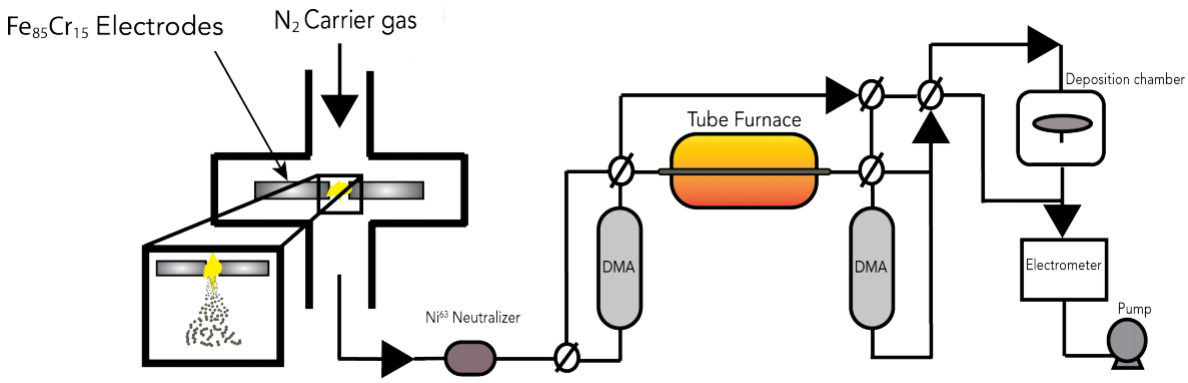

Figure 2.1: The schematics of SDG [13].

Figure 2.1 shows the schematic of the SDG; It consists of the spark chamber, charge neutralizer, sintering furnace tube, the differential mobility analyzer and finally the deposition chamber. The production process of nanoparticles start from the spark chamber. Two $Fe_{0.85}Cr_{0.15}$ electrodes are placed inside the chamber, a high voltage is applied to these electrodes and a spark is created in the gap between the electrodes. The spark then evaporates part of the electrode into small particles. The nanoparticles are transported through the system by means of a carrier gas, in this case ultra-pure nitrogen or nitrogen with the addition of hydrogen.

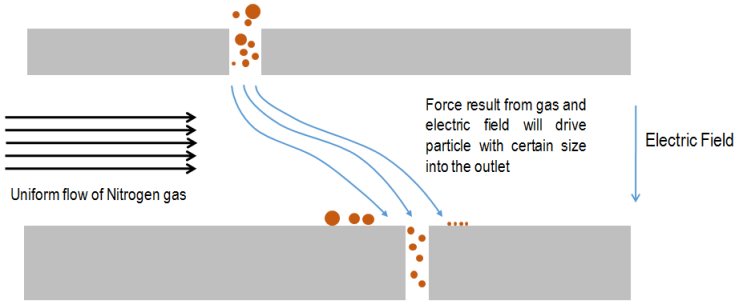

Figure 2.2: Working principle of DMA.

After generation, the nanoparticles will have an unknown charge distribution. To ensure a known charge distribution the particles are send through a beta-emitting Ni^{63} charger. A known charge distribution is of high importance for the size-selection step inside the differential mobility analyzers (DMA) [14].

The DMA is placed directly after the neutralizer, and this is where the first size selection of nanoparticles are taking place. The working principle of DMA is shown in figure 2.2. The selection of particles start when they enter the chamber with an applied electric field. Two forces are then acting on the particles, the force from the gas flow and the force from the electric field. Small particles are more affected by the electric filed than large particles, so by tuning the applied electric field, particles of a specific mobility diameter can be selected. For spherical particles, the mobility diameter is equal to the geometric diameter.

The size selected nanoparticles are then fed through a sintering tube furnace to

reshape into a more compact particle. In this project the particles were reshaped at 1100 C, which resulted in crystalline compact particles. To further narrow the size distribution, the sintered particles are fed through a second DMA. Finally, the nanoparticles are deposited onto a substrate inside the deposition chamber and exposed to air.

From the previous study [13], the nanoparticles produced by this method have shown to have a single crystalline structure and uniform shape. Figure 2.3 shows the TEM image of the particle, and indicate that the the nanoparticle formed is $(Fe_{0.85}Cr_{0.15})_xO_y$.

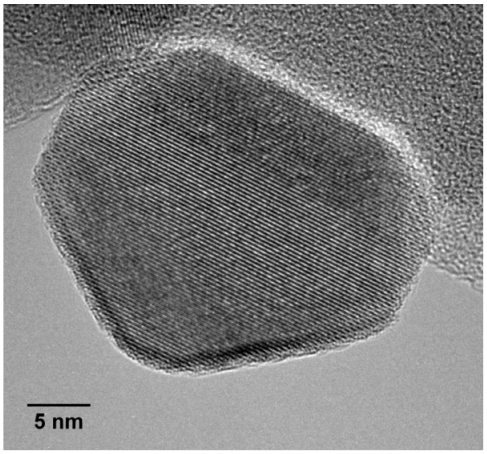

Figure 2.3: TEM of nanoparticle FeCr produced by SDG [13].

2.2 Scanning Electron Microscope

Scanning electron microscope (SEM) is an imaging technique used to study the morphology of the surface with a nano-scale structure. As the name suggests, the interaction between the electrons from the beam and the electrons from the surface are used to form an image. By scanning the beam across the entire surface, the entire surface can be mapped.

SEM as a particle based imaging technique is more advantageous to use as nanoscale imaging tools, compare to light based microscope due to the difference in resolution. The optical microscopy for example use visible light to do imaging, the smallest object distinguishable for this method is 200 nm, below that the image become blur due to interference of light. On the other hand the SEM system used accelerated electron to image nanostructure. The energy used to accelerate electron usually at 10-15 KV, the De broglie wavelength of electron is considerably low around 1-2 nm, with such short wavelength nanoscale structure image can be captured.

The working principle of SEM described at figure 2.4. The imaging process is started by accelerating the electrons with desired voltage. Then the electromagnetic lenses focus the beam towards an area on the surface. The scattered electron then is captured by a detector designed as a grid. Each square of the grid contain a single electron detector capable of detecting the presence of electrons. The detector sends

the reading of grid as a whole to the processing unit, where it is translated into differences in contrast, and finally forms the image of surface.

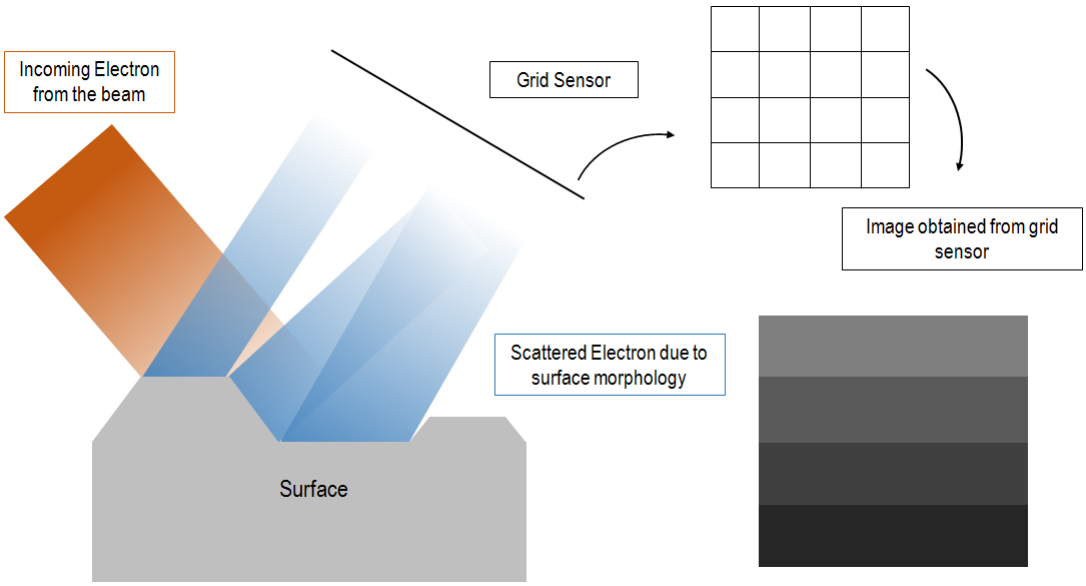

Figure 2.4: Simplified working principle of SEM.

The electron beam from the SEM can interact with the sample in different ways and give rise to both backscattered and secondary electrons, as shown in figure 2.5. Backscattered electrons are electrons from the beam that are elastically scattered by the sample and change their trajectory, but keep their energy. The backscattered electrons can be detected by a specific detector and can give information about morphology and some information about the elements in the sample.

The other type of interaction between the electrons from the beam and the sample gives rise to so called secondary electrons. The incoming electrons lose some of their energy to the electrons in the sample that are ionized, and form the secondary electrons. The secondary electrons are detected by a different detector and give information about the topography of the sample. The SEM used in this project is equipped with both a secondary electron and a backscattered electron detector and both imaging modes have been used to give complementary information about the studied surfaces.

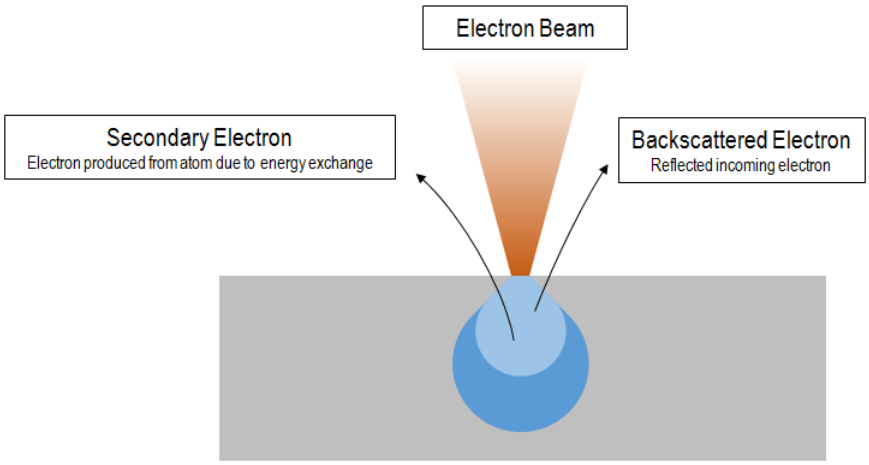

Figure 2.5: Interaction between the incoming electrons and the surface.

In SEM imaging, the edge of a structure is one of the most important features due to the extra contrast it gives. Figure 2.6 shows why an edge give a larger contribution to the contrast compared to the flat surface. The edge in a structure naturally has a larger surface area than a flat plane. Therefore, the incoming electrons has a larger area to interact with resulting in a larger number of scattered electrons for the detector to measure and hence more contrast in the image. Due to the edge, the number of electrons produced by the secondary process also increases. The surface at the edge provides a new escape route for secondary electron formed deep inside the surface and hence more secondary electrons are detected enhancing the contrast [15].

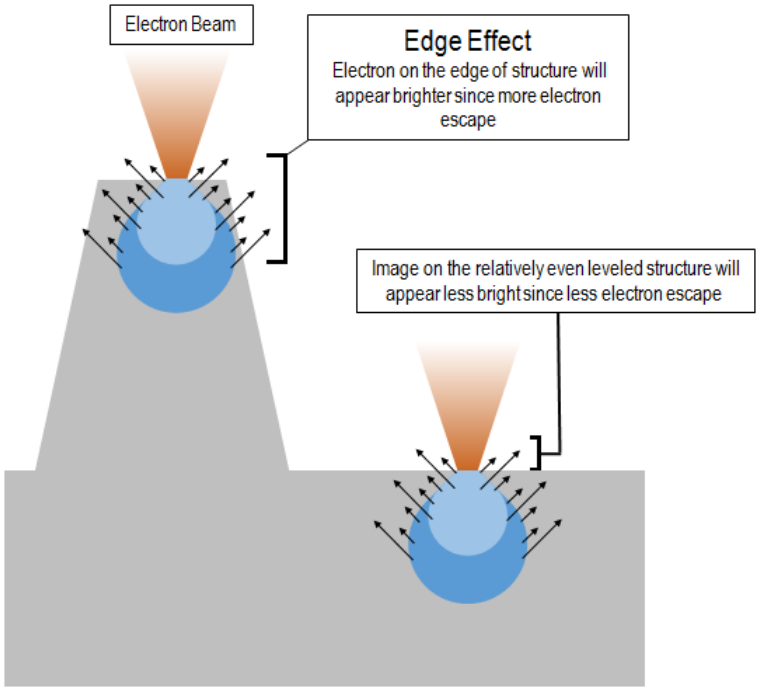

Figure 2.6: Edge effect on the surface that makes it appear brighter in the image.

The Scanning electron microscope is an extremely reliable technique to map the

morphology of surface structure. In this particular research project, SEM will be used to study the distribution and the coverage of the nanoparticles on the sample. The image will directly correlate with the real size of of the nanoparticles and the number of particles can be observed for every unit of area.

2.3 SQUID Magnetometer

SQUID or Superconductor quantum interference device is an ultra-sensitive magnetometer that able to detect trace of weak magnetic field. The superconductivity is a unique material state that occurs when low temperature is subjected. In this condition, electrons is coupled with each other and form a Cooper pair, which has property of a boson; a particle that has integer spin and does not obey Pauli exclusion property. The SQUID consists of a superconducting ring with two Josephson junctions, as shown in figure 2.7. The superconducting current I described by a wavefunction Ψ is split up along the two paths a and b ($I = I_a + I_b$), and then recombines again. As the wavefunctions Ψ_a and Ψ_b travels along the two paths a and b, they tunnel through the Josephson junctions and experience a phase shift determined by the magnetic flux threading the superconducting ring. As the two wavefunctions recombine, they are in phase and interfere constructively when the total magnetic flux Φ threading the ring is an integer time the flux quanta $\Phi_0 = 2 \times 10^{-15}$ Tm^2. Since the wavefunctions are describing all cooper pairs and thereby the total macroscopic supercurrent along the paths a and b, the supercurrent across the SQUID loop will also vary with a periodicity given by the flux quanta.

$$I_s \propto \left| \cos\left(2\pi \frac{\Phi}{\Phi_0} \right) \right| \tag{2.1}$$

During operation, variations in the supercurrent are determined by measuring the voltage across the SQUID circuit. The SQUID is thus an ultra-sensitive flux to voltage converter.

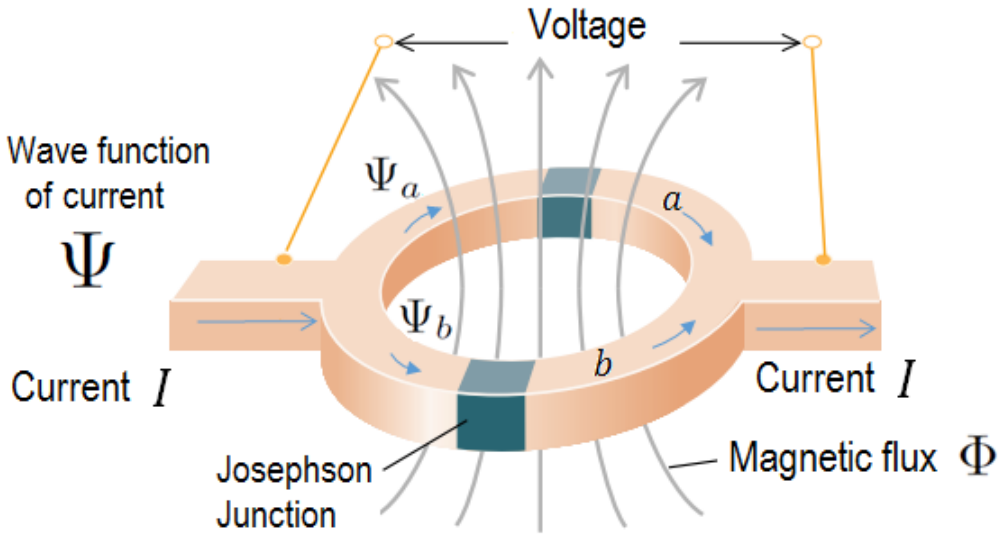

Figure 2.7: Two Josephson junction in a loop forming superconductor quantum interference device SQUID [16].

Chapter 3

Result and Discussion

In this chapter result of experiment will be described and discussed. The SEM image is used to study the size distribution and coverage of nanoparticles. The image is taken from different parts of sample, then the size of each particle is counted along their spread in an area. The analysis reveals single-domain sized particles and also estimation of nanoparticles coverage on the surface. A magnetometer equipped with a superconducting quantum interference device (SQUID) is used to measure magnetic characteristics of the sample. At a given magnetic field, the magnetization of the sample takes a value determined by the equilibrium between two opposing effects; the alignment along the magnetic field due to Zeeman interaction and the randomization from thermal fluctuations. The rate at which the moments flip due to thermal fluctuations is proportional to $e^{\Delta E/k_B T}$ where $\Delta E = KV$ is the anisotropy barrier. Thus, the larger the temperature the higher the thermal fluctuations. In order to study this dynamic, the measurement is done under two different protocol, first the magnetic field is set to be constant and the temperature is varied from 2 to 400 K, and second the temperature is set to be constant while external magnetic field is varied.

3.1 Size Distribution and Coverage of Nanoparticles

Figure 3.1 shows the images from several spots of the surface; the nanoparticle are deposited on top of a quartz surface. Due to the nature of substrate that is not conducting and considering how small the particle are, an image enhancement must be done. A thin layer of platinum and palladium are deposited onto the surface using atomic layer deposition. The thickness of this layer is 3 nm and it covers the surface uniformly. The diameter of the nanoparticle are expected to grow due to the extra layer; some adjustment is made during data tabulation to obtain the real value.

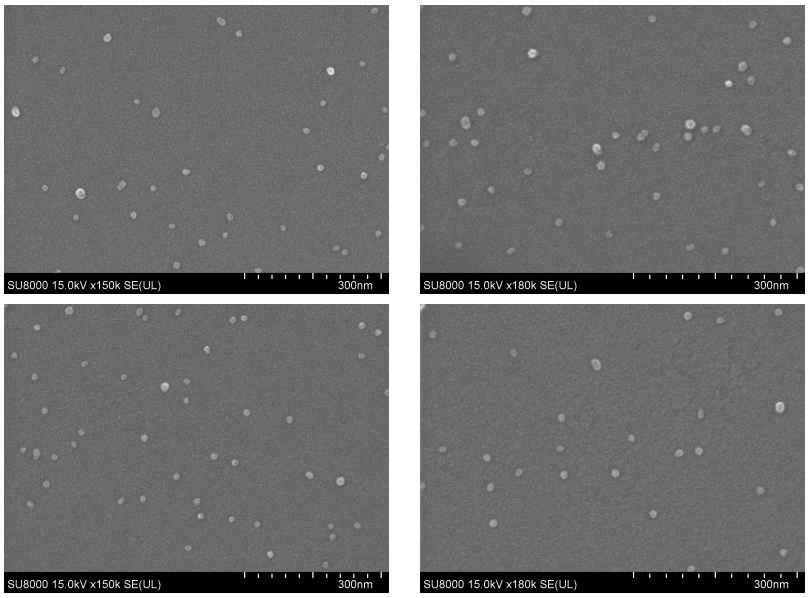

Table 3.1: SEM images of nanoparticles on various spots on the sample.

The size distribution study is done by measuring the diameter of the nanoparticles in the images and making a histogram out of it. Figure 3.1 shows the normalized distribution of nanoparticle diameter. While the majority of the nanoparticles have a diameter of 9-12 nm, a small percentage of them varied around 16-18 nm, and some of them are even smaller, around 6 nm. This data shows that the sample consists of desired nanoparticle size and furthermore guarantee that the particles are in a single-domain magnet configuration. From all of the images, one can estimate the particle coverage on the sample; it is defined as the area needed to find exactly one particle. The coverage turns out to be 10404 nm^2/one particle, in average the particle has 102 nm distance between each other.

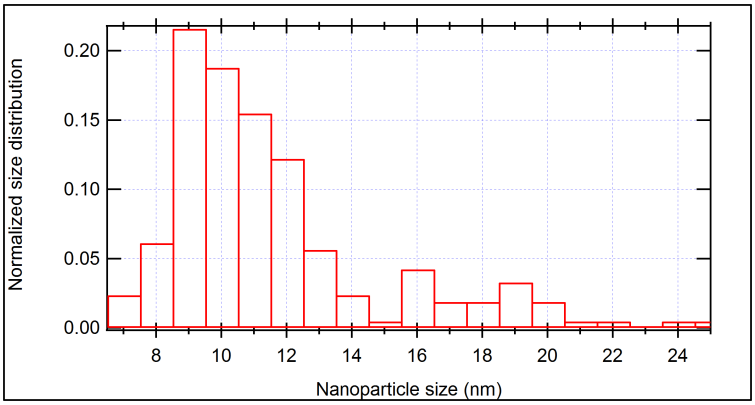

Figure 3.1: Distribution of nanoparticle size found on the sample.

The distribution and coverage study reveal that in the area of 10404 nm^2 a particle can be found. The maximum dipole-dipole interaction between two particles separated by the average distance of 102 nm can be estimated using the magnetic moments obtained in appendix A, which is 3532 μ_B and equation 1.4. Figure 3.2 shows the approximate coverage of nanoparticles.

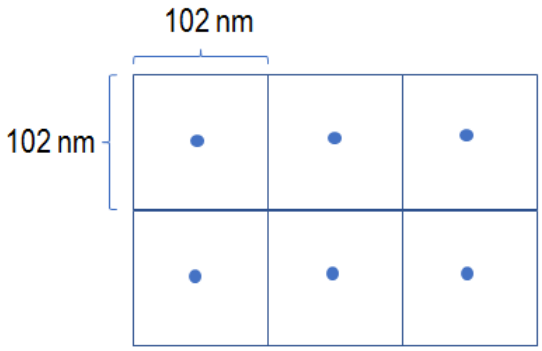

Figure 3.2: Nanoparticle coverage model.

In this estimation we assume the condition of maximum interaction, the interacting magnetic moment is parallel to each other and the angle between position vector $\vec{r}$ and magnetic moment vector $\vec{\mu}$ is 90°, the vector representation shown by figure 3.3.

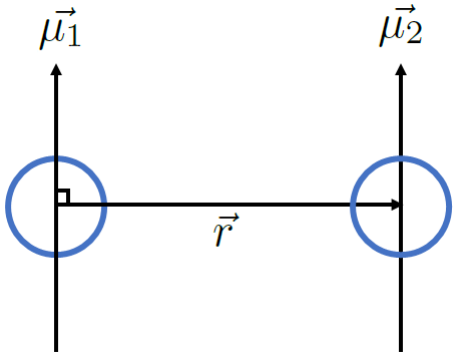

Figure 3.3: Vector representation of maximum dipole-dipole interaction.

This condition will make :

$$\vec{\mu} \cdot \vec{r} = |\mu||r| \cos(90^\circ) = 0. \tag{3.1}$$

The maximum dipole-dipole interaction energy is written as:

$$E_{max} = \frac{\mu_0}{4\pi r^3}[\vec{\mu_1} \cdot \vec{\mu_2}] = \frac{\mu_0}{4\pi r^3}\mu_1\mu_2 \tag{3.2}$$

The maximum dipole-dipole energy is then:

$$\begin{aligned} E_{max} &= \frac{\mu_0}{4\pi r^3}\mu_1\mu_2 \\ &= \frac{1.24 \times 10^{-6}}{12.56 \times (102 \times 10^{-9})^3}(3532 \times 9.27 \times 10^{-24})^2 J \\ &= 1.01 \times 10^{-25}\ J = 6.3 \times 10^{-7}\ eV \end{aligned} \tag{3.3}$$

The estimated dipole-dipole energy is very low, therefore one can assume that the inter-particle interactions have been successfully minimized.

3.2 SQUID Result and Discussion

The first SQUID result that will be discussed is the temperature dependence of the nanoparticle magnetic moments at a fixed external magnetic field of 100 mT. The data was obtained by using the following protocol, the sample is cooled down from room temperature to 2 K, then the magnetometer start recording the moment while sample is being heated up to 400. After it reached 400 K, the sample is cooled down again to 2 K.

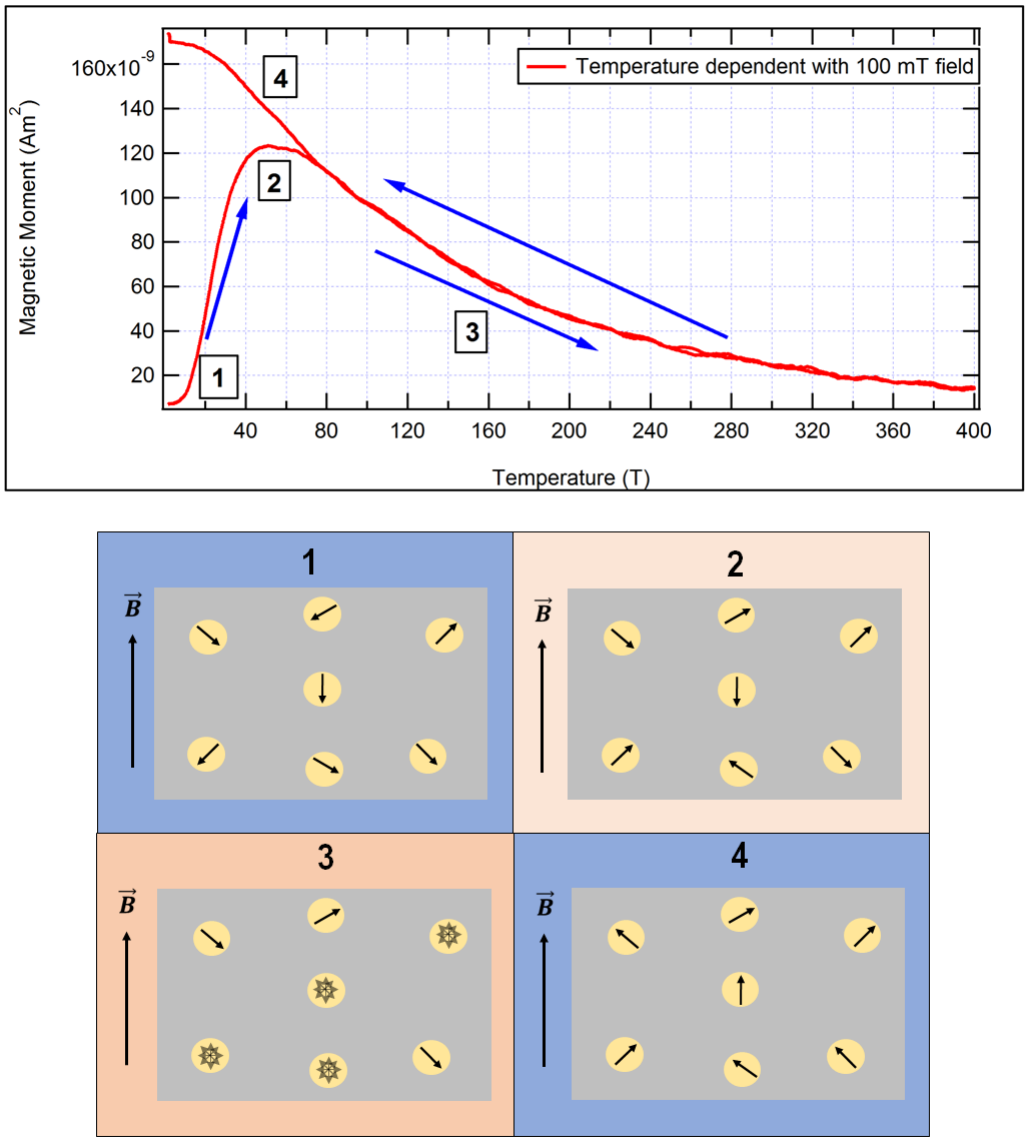

Figure 3.4: The magnetic moment as the function of temperature. The dynamics of magnetic moment is describe with corresponding image below the data. The yellow circle represent nanoparticle, the arrow inside is the magnetic moment, while the multi-directional arrow represent random orientation of magnetic moment, and the gray area is the substrate.

Figure 3.4 shows the result of the temperature dependence of the magnetic moment of the sample and a schematic representation of the magnetic dynamic that happen at measurement. Each number denotes different dynamics corresponding to the image below. Chronologically the dynamic can be explained as follows.

1. At room temperature, the thermal energies are much larger than the anisotropy barrier and the orientation of the magnetic moments will flip randomly. As the temperature is cooled down from room temperature to 2 K, the fluctuating individual moments of the particle are randomly frozen. At 2 K an external magnetic of 100 mT is applied.

2. At low temperatures, the thermal energies are not large enough for the system to adopt an equilibrium magnetization during the time scale of the experiment and the system is said to be in a blocked state. As the temperature increase, the thermal energy becomes higher, and it becomes easier to align the moments with the external field ($\vec{\mu} \cdot \vec{B} > 0$) and the magnetization increases and reaches a maximum at $T_B \sim 51.1$ K. This temperature is defined as the blocking temperature T_B, the temperature at which the rate of thermal fluctuations are comparable with the measurement time.

3. The thermal energy keeps rising and and is increasingly dominating over the alignment due to the Zeeman energy. As the result, the magnetization decreases with increasing temperature. From this point, the cooling down process is started.

4. When the sample is cooled down again in a magnetic field, the system has time to reach equilibrium, and the magnetization increases as the temperature is lowered, and the thermal fluctuations decrease.

There are several key points can be highlighted from the measurement. The thermal influence over nanoparticle is divided into two different temperature regions. Below the blocking temperature, the magnetic moment seems to be frozen and the system can not reach an equilibrium magnetization. At temperature above the blocking temperature ($T_B \simeq 51$K) the system can adopts an equilibrium magnetization given by the thermal energies and the interaction with the external magnetic field. This situation is similar to that with a paramagnetic atom system, with the difference that the magnetic moment now is made up of thousands of individual moments. Because of the analogy to the paramagnetic case, the system is said to be in a superparamagnetic state at temperatures above the blocking temperature.

As demonstrated above temperature hold significant effect on the response of particle. The second experiment is trying to measure the response of the magnetic moment to external magnetic field changes. Magnetization curve characterization is performed on the particles with the applied field cycle of 7 to -7 T.

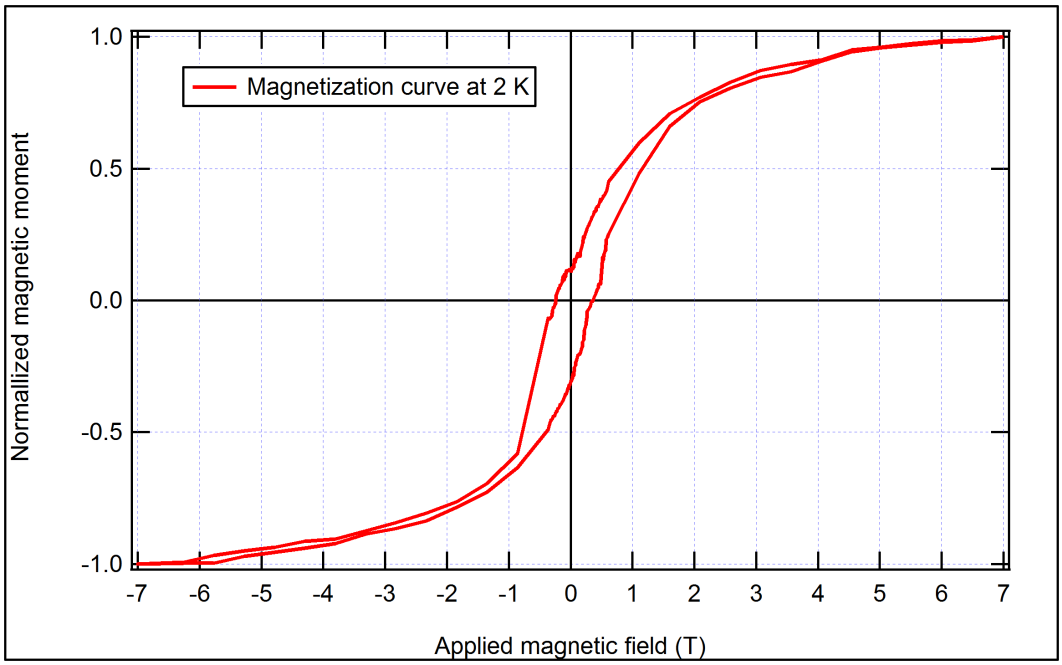

Figure 3.5: The Magnetization curve of nanoparticle at 2 K

The magnetization curve shows hysteresis similar to that of a permanent magnet with coercive field of approximately 25 mT. This phenomena can be explained by examining the state the particle is under experimental condition. At 2 K, the particle is in a blocked state ($T < T_B$), which means that the thermal energies are not sufficient to reach equilibrium during the time scale of the experiment. After being magnetized in a large magnetic field, the response to external magnetic field changes are slow compared to the measurement time, and the system exhibits hysteresis. If the sample were not in a blocked state ($T > T_B$) the system would have time to reach equilibrium and the magnetization curve would be similar to that in Figure 1.5.

It is difficult to compare these results with published data since there are no published measurements on this fully oxidized single-crystalline $Fe_{85}Cr_{15}$ structure. The magnetic properties of nanoparticles also depend on the degree of dipole-dipole interaction between the nanoparticles. Increased dipole interaction can lead to an increased blocking temperature and coercive field. The observed coercive field of $\sim$ 25 mT is similar to that of 27.8 mT observed for 11.6 nm Fe_3O_4 nanoparticles [17]. However, in this study, the dipole interactions were significant, and they observed a blocking temperature of $T_B = 263.6$ K. In the same study, 6.6 nm Fe_3O_4 nanoparticles were diluted in paraffin which resulted in a decrease of the blocking temperature from 203 K to 108 K. One should also keep in mind that the blocking temperature dependence on the time scale of the experiment. In our case, the addition of 15 % Cr will also influence the magnetic properties of the system.

Chapter 4

Conclusion

The Iron-chrome oxide nanoparticle as alloy test system is successfully fabricated. SEM image reveals the size distribution of nanoparticle size, the majority of particle lies in the range of 9 to 12 nm. The coverage of deposition is shown to be 10404 nm^2/particle. Estimating the dipole-dipole interaction between two neighboring particles gives a value of 6.3×10^{-7} meV which demonstrate that this interaction is small.

Furthermore, it is demonstrated that a magnetometer equipped with a SQUID can detect the magnetic signal from this diluted sample. Temperature dependent measurements show that the system is superparamagnetic with a blocking temperature of $T_B = 51$ K. When nanoparticle subjected to the temperature above the blocking temperature, it exhibits Superparamagnetic state, magnetic state that has similarity with paramagnet. Under the blocking temperature the nanoparticle experiencing blocked state where the magnetic moments are frozen during the time scale of the experiment and appear to behave similarly to a ferromagnet.

The magnetization curve reveals the response of material under external magnetic field at 2 K. At 2 K, the system is in a blocked state and cannot adopt an equilibrium magnetization during the time scale of the experiment. Consequently, the magnetization curve shows hysteresis similar to that of a permanent magnet.

However, the low signal lead to difficulties measuring magnetization curves. Future systems will exhibit much larger magnetic moments and thus larger signal, but this will also lead to larger inter-particle interactions. Considering that the present interactions were very small, there is room for increasing the magnetic moments of the particles and still have small interparticle interactions. With the same average distance as the present sample, an increase of the particle magnetic moment with a factor of 10 would only lead to a dipole interaction of about 500 mK. Additionally, there is also room for improving the sample holders and thereby increasing the signal to noise ratio.

Appendix A

Magnetization in FeCr Oxide Nanoparticles

The FeCr oxide has the chemical formula of $(Fe_{0.85}Cr_{0.15})_3O_4$, one can calculate the magnetization of this system can be done by applying formula in 1.6. Since magnetization is heavily dependent on the volume of material we assume that the system is in nanoparticle with perfect spherical shape and radius 5 nm.

$$V_{nanoparticle} = \frac{4}{3}\pi r^3 = \frac{4}{3}\pi(5 \times\ 10^{-9}m)^3 = 5.24 \times 10^{-25}m^3 \tag{A.1}$$

The $(Fe_{0.85}Cr_{0.15})_3O_4$ unit cell is a cube with edge length of 0.84 nm and its volume is:

$$V_{unit\,cell} = a^3 = (0.84 \times 10^{-9})^3 = 5.93 \times 10^{-28}m^3. \tag{A.2}$$

The amount of unit cell in nanoparticle is then:

$$N = \frac{V_{nanoparticle}}{V_{unit\,cell}} = \frac{5.24 \times 10^{-25}m^3}{5.93 \times 10^{-28}m^3} = 883. \tag{A.3}$$

Inside the nanoparticle with 10 nm diameter there are 883 unit cell of $(Fe_{0.85}Cr_{0.15})_3O_4$. In the unit cell there are two Fe^{+3} ion with opposing magnetic moment, 15% of Fe^{+3} is substituted by The Cr^{+} ion. Both Cr^{+} and Fe^{3+} exhibit identical magnetic moment since they have same electronic structure as shown in figure A.1, and leaving Fe^{+2} ion as the only contributor for magnetic moment of the system with the magnitude of $4\mu_B$ [18].

$$N_{Fe^{+2}} = 883. \tag{A.4}$$

The magnetic moment for each individual nanoparticle therefore:

$$\mu = 883 \times 4\mu_B = 3532\mu_B \tag{A.5}$$

Now we apply equation 1.6.

$$\begin{aligned} M = N\mu(\coth x - \frac{1}{x}) = 3532\mu_B(\coth x - \frac{1}{x}) \\ with \\ x = \frac{4\mu_B \times B}{k_B T} \end{aligned} \tag{A.6}$$

The magnetic field is set to have fixed range from -2 to 2 T, while the temperature is varied with 100 K, 200, and 300 K.

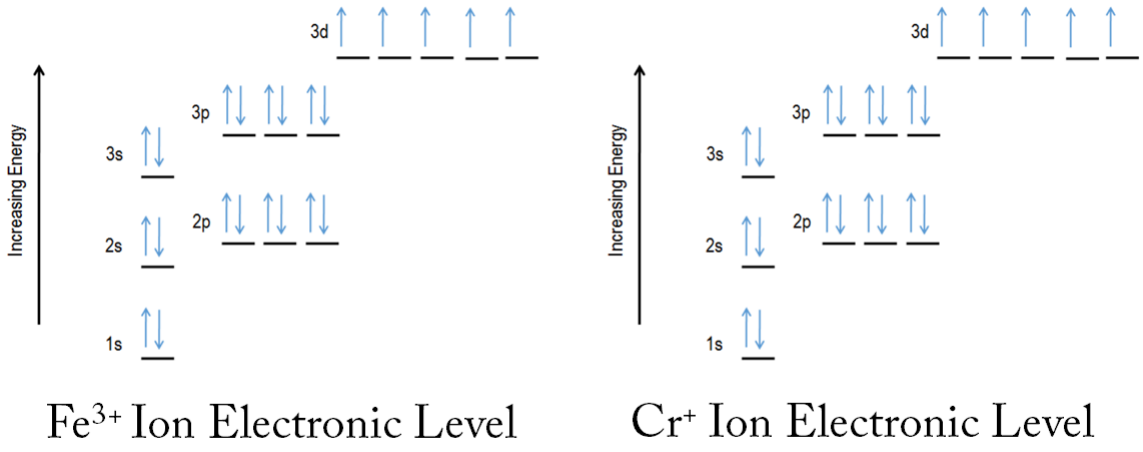

Figure A.1: Electronic structure of Fe^{3+} and Cr^{+} ion.

Bibliography

[1] L. Blaney, "Magnetite (fe3o4): Properties, synthesis, and applications," 2007.

[2] Y. Wang, C. Xu, Y. Chang, L. Zhao, K. Zhang, Y. Zhao, F. Gao, and X. Gao, "Ultrasmall superparamagnetic iron oxide nanoparticle for t 2-weighted magnetic resonance imaging," *ACS applied materials & interfaces*, vol. 9, no. 34, pp. 28959–28966, 2017.

[3] M. Mahmoudi, S. Sant, B. Wang, S. Laurent, and T. Sen, "Superparamagnetic iron oxide nanoparticles (spions): development, surface modification and applications in chemotherapy," *Advanced drug delivery reviews*, vol. 63, no. 1-2, pp. 24–46, 2011.

[4] D. Zanella, E. Bossi, R. Gornati, C. Bastos, N. Faria, and G. Bernardini, "Iron oxide nanoparticles can cross plasma membranes," *Scientific Reports*, vol. 7, no. 1, p. 11413, 2017.

[5] N. Poudyal and J. P. Liu, "Advances in nanostructured permanent magnets research," *Journal of Physics D: Applied Physics*, vol. 46, no. 4, p. 043001, 2012.

[6] J. Estelrich, E. Escribano, J. Queralt, and M. A. Busquets, "Iron oxide nanoparticles for magnetically-guided and magnetically-responsive drug delivery," *International journal of molecular sciences*, vol. 16, no. 4, pp. 8070–8101, 2015.

[7] A. P. Guimarães and A. P. Guimaraes, *Principles of nanomagnetism*, vol. 7. Springer, 2009.

[8] S. Bedanta and W. Kleemann, "Supermagnetism," *Journal of Physics D: Applied Physics*, vol. 42, no. 1, p. 013001, 2008.

[9] R. Carey and E. D. Isaac, "Magnetic domains and techniques for their observation," 1966.

[10] Q. Li, C. W. Kartikowati, S. Horie, T. Ogi, T. Iwaki, and K. Okuyama, "Correlation between particle size/domain structure and magnetic properties of highly crystalline fe 3 o 4 nanoparticles," *Scientific Reports*, vol. 7, no. 1, p. 9894, 2017.

[11] S. Schwyn, E. Garwin, and A. Schmidt-Ott, "Aerosol generation by spark discharge," *Journal of Aerosol Science*, vol. 19, no. 5, pp. 639–642, 1988.

[12] M. E. Messing, "The advantages of spark discharge generation for manufacturing of nanoparticles with tailored properties," *Journal of Green Engineering*, vol. 5, no. 4, pp. 83–96, 2015.

[13] B. M. M. M. R. W. M. M. C. Preger, L.Ludvigsson, "Controlled generation of alloyed ferrous nanoparticles for future magnetic materials," *Poster presented at the 2017 European Aerosol Conference, Zurich, Switzerland*, 2017.

[14] M. E. Messing, R. Westerstrom, B. O. Meuller, S. Blomberg, J. Gustafson, J. N. Andersen, E. Lundgren, R. van Rijn, O. Balmes, H. Bluhm, *et al.*, "Generation of pd model catalyst nanoparticles by spark discharge," *The Journal of Physical Chemistry C*, vol. 114, no. 20, pp. 9257–9263, 2010.

[15] J. I. Goldstein, D. E. Newbury, J. R. Michael, N. W. Ritchie, J. H. J. Scott, and D. C. Joy, *Scanning electron microscopy and X-ray microanalysis*. Springer, 2017.

[16] J. Clarke, "Squids," *Scientific American*, vol. 271, no. 2, pp. 45–53, 1994.

[17] D. Caruntu, G. Caruntu, and C. J. O'Connor, "Magnetic properties of variable-sized fe3o4 nanoparticles synthesized from non-aqueous homogeneous solutions of polyols," *Journal of Physics D: Applied Physics*, vol. 40, no. 19, p. 5801, 2007.

[18] M.-H. Phan, J. Alonso, H. Khurshid, P. Lampen-Kelley, S. Chandra, K. Stojak Repa, Z. Nemati, R. Das, Ó. Iglesias, and H. Srikanth, "Exchange bias effects in iron oxide-based nanoparticle systems," *Nanomaterials*, vol. 6, no. 11, p. 221, 2016.